Natural Resources Canada
Ressources naturelles Canada

From mid-plate to subduction zone: stratigraphy of the northeast Juan de Fuca plate, offshore British Columbia

K.M.M. Rohr, H. King, M. Riedel, and U. Schmidt

Geological Survey of Canada
Current Research 2019-4

2019

Canada

Geological Survey of Canada
Current Research 2019-4

From mid-plate to subduction zone: stratigraphy of the northeast Juan de Fuca plate, offshore British Columbia

K.M.M. Rohr, H. King, M. Riedel, and U. Schmidt

2019

ISSN 1701-4387
ISBN 978-0-660-32100-4
Catalogue No. M44-2019/4E-PDF
https://doi.org/10.4095/314906

A copy of this publication is also available for reference in depository libraries across Canada through access to the Depository Services Program's Web site at http://dsp-psd.pwgsc.gc.ca.

This publication is available for free download through GEOSCAN (http://geoscan.nrcan.gc.ca).

Recommended citation

Rohr, K.M.M., King, H., Riedel, M., and Schmidt, U., 2019. From mid-plate to subduction zone: stratigraphy of the northeast Juan de Fuca plate, offshore British Columbia; Geological Survey of Canada, Current Research 2019-4, 14 p. https://doi.org/10.4095/314906

Critical review

R. Enkin

Authors

K.M.M. Rohr (Kristin.Rohr@canada.ca)
Geological Survey of Canada
9860 West Saanich Road
Sidney, British Columbia
V8L 4B2

H. King (Heather.King@canada.ca)
Geological Survey of Canada
3303 33 Street Northwest
Calgary, Alberta
T2L 2A7

M. Riedel (mriedel@geomar.de)
GeoMAR Helmholtz Centre for Ocean Research Kiel
Wischhofstr. 1-3 D-24148
Kiel, Germany

U. Schmidt
Retired

Correction date:

From mid-plate to subduction zone: stratigraphy of the northeast Juan de Fuca plate, offshore British Columbia

Rohr, K.M.M., King, H., Riedel, M., and Schmidt, U., 2019. From mid-plate to subduction zone: stratigraphy of the northeast Juan de Fuca plate, offshore British Columbia; Geological Survey of Canada, Current Research 2019-4, 14 p. https://doi.org/10.4095/314906

Abstract: Quaternary sedimentary stratigraphy in Ocean Drilling Program site 1027 was tied to three regional multichannel seismic reflection profiles across the northeastern Juan de Fuca plate to the Cascadia subduction zone. A velocity gradient from a refraction study provided a good fit to convert depth of stratigraphic horizons to two-way traveltime. Topography of basement ridges prevents correlating time horizons older than 0.76 Ma on a regional scale on seismic reflection sections. By that time sediments had filled almost to the top of basement ridges and deposition of the Nitinat fan had begun. After 0.46 Ma, coarser sediments and debris flows were deposited from the fan into the seaward reaches of Cascadia Basin, and above the 0.28 Ma time horizon, the reflection character of deposits around the fan is that of poorly sorted mass-transport deposits with intermittent layering. More than half of the sediments in the trench are from the Nitinat fan; they are approximately 2 Ma younger than previously thought. Growth faults created by bending stresses from the sediment load and subduction are primarily observed in intervals that predate the Nitinat fan and accumulated at slower sedimentation rates. These faults appear to be utilizing extensional faults that are part of the original fabric of the igneous crust.

Résumé : La stratigraphie sédimentaire du Quaternaire au site 1027 du Programme de sondage des fonds marins a été calée sur trois coupes régionales de sismique-réflexion multicanal qui traversent la partie nord-est de la plaque Juan de Fuca et se prolongent jusqu'à la zone de subduction de Cascadia. Un gradient de vélocité tiré d'une étude de sismique-réfraction a permis un bon ajustement de la profondeur des horizons stratigraphiques au temps de trajet double. La topographie des crêtes du socle empêche la corrélation régionale des horizons chronostratigraphiques antérieurs à 0,76 Ma dans les coupes de sismique-réflexion. À cette époque, l'accumulation de sédiments avait presque atteint le sommet des crêtes du socle et le dépôt du cône Nitinat avait commencé. Après 0,46 Ma, des sédiments plus grossiers et des coulées de débris en provenance du cône ont été déposés dans les parties extérieures du bassin de Cascadia et, au-dessus de l'horizon chronostratigraphique de 0,28 Ma, le caractère de la réflexion associée aux dépôts situés au pourtour du cône est celui de dépôts de transport de masse mal triés présentant une stratification intermittente. Plus de la moitié des sédiments dans la fosse proviennent du cône de Nitinat; ils sont plus jeunes d'environ deux millions d'années qu'on ne l'avait pensé. Des failles synsédimentaires résultant des contraintes de flexion liées à la surcharge sédimentaire et à la subduction sont principalement observées dans des intervalles qui sont antérieurs à la formation du cône de Nitinat et se sont accumulés suivant des taux de sédimentation plus faibles. Ces failles semblent emprunter la trace de failles d'extension qui font partie de la fabrique originale de la croûte ignée.

INTRODUCTION

Although many thousands of kilometres of reflection profiles have been collected across the Juan de Fuca plate, there is no regional seismic stratigraphic framework. Sedimentary fill in the Cascadia Basin (Fig. 1) has long been known to consist of Pleistocene turbidites over Neogene hemipelagic sediments (Ewing et al., 1968; Hayes and Ewing, 1970, McManus et al., 1972; Davis and Hyndman, 1989), but actual dates on horizons were not obtained until 1997. During the Ocean Drilling Program (ODP) Leg 168, a suite of holes on the Juan de Fuca plate were drilled into the sedimentary section above igneous crust that ranges in age from 0.86 to 3.59 Ma (Shipboard Scientific Party, 1997a). Dates on sedimentary horizons were correlated with local seismic-reflection lines (Zühlsdorff and Spiess, 2001; Underwood et al., 2005), but not extended to a regional scale.

In this study we tie sedimentary stratigraphy of cores from the oldest drill site of Leg 168, on 3.59 Ma igneous crust, to three regional multichannel seismic reflection lines in order to estimate ages of sediments in the reflection data. Depth in cores is related to time in seismic reflection profiles by using seismic velocities of the sediments. Sediments above younger basaltic crust are from somewhat different

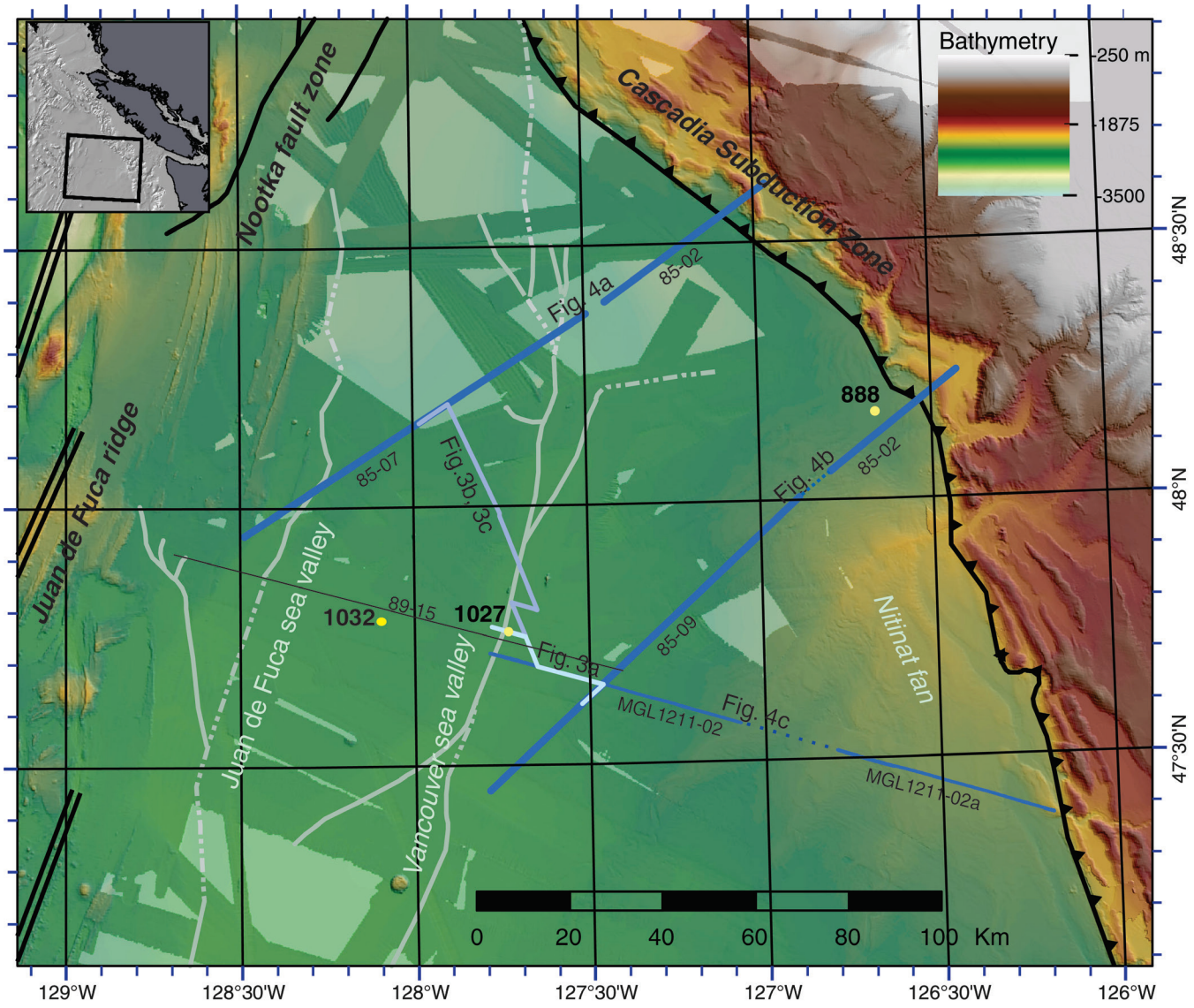

Figure 1. Northeastern Juan de Fuca plate. Bathymetry is based on a collection of multibeam surveys and transit lines compiled by Ryan et al. (2009) and downloaded from http://www.geomapapp.org. Underlying it is regional bathymetry compiled by Natural Resources Canada and Canadian Hydrographic Service. Reflection lines in Figures 3 and 4 are shown as light and dark blue lines, respectively. Boundaries between tectonic plates are shown in black; the thrust fault denotes the deformation front of the Cascadia subduction zone. Sea valleys are shown in grey based on Hampton et al. (1989) and Karl et al. (1989) and updated here using better known bathymetry. Solid lines indicate identification from multibeam data and dashed lines are based on regional bathymetry. Ocean Drilling Program sites are shown as yellow dots.

depositional regimes and we do not consider them here. Previous work tied the top 150 m of sediments to local reflection lines over younger igneous crust; here we extend that work to older sediments and to a regional scale. Two velocity functions, one derived from multichannel seismic reflection data (Davis et al., 1992; Rohr et al., 1992) and the other from an ocean-bottom seismometer refraction study (Horning et al., 2016) provide good ties between the cores and a coincident reflection section. We correlated the dated horizons through a network of single-channel reflection lines to connect to the multichannel lines. Basement ridges affected the flow of turbidite sediments (Zühlsdorff and Spiess, 2001; Underwood et al., 2005; Zühlsdorff et al., 2005); we have tracked three horizons that lie largely above the highest parts of basement ridges: the base of the Nitinat fan (0.76 Ma) and two younger horizons in the fan that mark the onset of sandier deposition (0.46 Ma) and abundant debris flows (0.28 Ma). These dates can provide constraints for elastic modelling of plate flexure and thermal studies of mechanical structure of the subducted oceanic plate. This study shows that seemingly reasonable assumptions about sedimentation processes can be significantly in error, and that sampling and dating the sedimentary section is a crucial part of constraining regional geological and geophysical processes. Although mathematical models of the Cascadia subduction zone are increasingly sophisticated and incorporate many variables, to date they have been based on simplistic assumptions of sedimentation processes and rates.

REGIONAL GEOLOGY

The Cascadia sedimentary basin lies on the Juan de Fuca plate between the Juan de Fuca spreading centre and Cascadia subduction zone (e.g. Gardner et al., 1993) (Fig. 1). The age of the igneous oceanic crust is well constrained by magnetic anomalies (Riddihough, 1977; Wilson, 1993) and only spans a 10 Ma range. As the crust cools, it sinks and as it is loaded by sedimentary fans originating from North America, it is further depressed. In addition, subduction of the plate under North America flexes and depresses the plate. A seismic reflection transect off Washington state found that 2900 m of total subsidence had occurred at the deformation front of the subduction zone; cooling comprised ~900 m of subsidence, the sediment load ~1200 m and subduction another ~800 m (Han et al., 2016). Cooling is in effect across the entire plate, a variable sedimentary load affects the plate up to 150 km from the trench, and subduction loading affects crust within 50 to 70 km of the trench (Han et al., 2016). Sedimentary thickness varies from centimetres on very young basalt up to 3 km in some parts of the trench (Han et al., 2017; Ferguson et al., 2018).

The dominant sedimentary processes in the basin are hemipelagic deposition and sediment-gravity flow (e.g. turbidity currents and debris flows). Upwelling along the continental slope promotes biological activity and hemipelagic deposition rates can be high: as much as 100 m/Ma (10 cm/ka.) (Su et al., 2000). The height of the spreading centre effectively traps turbidite deposits in the basin. Deposition rates were particularly high during glacial melt episodes in the Quaternary. Deep sea valleys and channels have been identified in the abyssal plain from bathymetry and sidescan sonar (Griggs and Kulm, 1973; Hampton et al., 1989; Karl et al., 1989; Underwood et al., 2005; Zühlsdorff et al., 2005); we have updated these identifications using multibeam data (Ryan et al., 2009; http://www.geomapapp.org) and regional bathymetry (Natural Resources Canada and Canadian Hydrographic Services) (Fig. 1). The sea valleys are about 10 km wide, whereas the channels in the outer Nitinat fan are about 1 km wide. The Juan de Fuca sea valley presently originates from the flanks of the spreading centre and the Vancouver sea valley originates in small canyons off central and northern Vancouver Island (Fig. 1). A number of meandering channels originate from the apex of Nitinat fan. The fan was initiated 0.76 Ma ago (Andrews et al., 2012) when the previous northward flow of the Fraser river was reversed and diverted to the Pacific Ocean.

A suite of holes was drilled through the sedimentary section into 0.86 to 3.59 Ma igneous crust by ODP to study the hydrogeology of the permeable basalt interval (Shipboard Scientific Party, 1997a). Examination of cores identified two main lithological units in the sediments: a lower unit (II) of hemipelagic mud and an upper unit (I) of turbidites interlayered with hemipelagic mud (Shipboard Scientific Party, 1997b) (Fig. 2). The transition between these units is time-transgressive because the youngest oceanic crust is elevated and received only hemipelagic sediments until it cooled and sank below the level of the prograding systems of turbidite deposition. The upper unit was further divided into an older subunit of silty turbidites and a younger subunit of coarser turbidites and debris flow deposits (Shipboard Scientific Party, 1997b).

Su et al. (2000) identified 11 biostratigraphic events in the Pleistocene by appearance or disappearance of key microfossils and computed average deposition rates for each interval between those events. In Site 1027 the 0.76 Ma horizon, onset of Nitinat fan deposition (Andrews et al., 2012), lies within subunit IB. Above it silty turbidites were deposited more frequently (Shipboard Scientific Party, 1997b); earlier silty turbidites could be distal flows from the Astoria fan, which is thought to have been active throughout the Quaternary (Prytulak et al., 2006). Deposition of coarser sandy turbidite layers (subunit IA) began at 0.46 Ma.

Studies of the drilled sediments found that significant hiatuses lie between the top of the basaltic crust and the first preserved sediments (Shipboard Scientific Party, 1997b; Su et al., 2000). The hiatuses range in duration from 0.1 to more than 1.7 Ma (Su et al., 2000); their origin is unknown, but could be from nondeposition or fast bottom currents eroding the first deposited sediments. The surface of the igneous crust is very irregular and includes numerous ridges that formed subparallel to the spreading centre; the ridges

formed in and around the spreading centre from the combination of volcanism and extensional faulting. These ridges are of sufficient height — several hundred metres — that they compartmentalized flow of turbidity currents into intervening valleys (Zühlsdorff and Spiess, 2001; Underwood et al., 2005; Zühlsdorff et al., 2005). A few seamounts that erupted either near or off the axis of the spreading centre are also present.

Lateral variability of sedimentary lithology, deposition rates, and recurrence intervals of turbidite deposition was noted between the ODP drill sites of Leg 168 across distances of 6 to 30 km (Underwood et al., 2005). Processes such as channel switching, overbank flow, local slumping and debris flows, as well as the number of different sedimentary sources likely contributed to this variability (Underwood et al., 2005).

A lack of velocity logs has hindered tying core-based lithostratigraphy to reflection sections; however, Zühlsdorff and Spiess (2001) tied the top 150 m of core in 6 sites up to 1.62 Ma in basement age using density logs and empirical velocity functions to calculate synthetic seismograms. They identified reflectors corresponding to lithological units IA and IB on coincident reflection records, but not the biostratigraphic units of Su et al. (2000). As a starting point, seismic velocity in the sediments was assumed to be 1500 m/s and was adjusted according to lithological and density-log character until the synthetic seismogram matched reflection data. This corresponds to the top 200 ms of reflection data. They tied lines locally to drill sites and found only one reflector that could be tied to more than one site over 22 km. Underwood et al. (2005) published a seismic reflection section with approximate ages on it for acoustic horizons between ODP sites 1026 and 1027, but did not pinpoint the exact two-way traveltime of the correlative stratigraphic horizons. At Site 1032 over 1.95 Ma basement, reliable velocity and density logs were obtained from 75 to 200 m below seafloor (bsf) (Shipboard Scientific Party, 1997c); *see* Methods section for more detail.

DATA

Single and multichannel seismic reflection data interpreted here range in age from 1985 (Davis et al., 1992) to 2012 (Han et al., 2016). These data were compiled during a regional review of geology to assess setting aside areas as marine conservation zones (Ferguson et al., 2018). Data collected in 1995 and 1996 were published by Rosenberger et al. (2000), lines 85-01 and 85-02 by Davis and Hyndman (1989), lines 85-07 and 85-09 by Hasselgren and Clowes (1995), and MGL1112-02 was published by Han et al. (2016). Lines 85-07 and 85-09 were re-processed (Ferguson et al., 2018) following the approach of Hasselgren and Clowes (1995) because digital data files of the migrated stacks could not be located. With modern interactive software for picking stacking velocities, we expect the sedimentary section is better imaged. This is the first time that the 1985 lines across the basin and the trench have been displayed together as composite lines showing the flexure of the young plate into the Cascadia subduction zone.

The 1988 survey was only recorded on paper sections; these were scanned and vectorized into SGY files for digital interpretation. These files allow interpretation of time, but have limited amplitude information. Surveys that intersect did not always match in seafloor arrival time partly because of navigation errors, but also because of different acquisition systems. To aid interpretation, start times of lines were adjusted to better align the seafloor reflection time; the amount of the adjustment was typically less than 50 ms. Small errors were tolerated.

Frequency content differed between the surveys: the original 8809 survey ranged from 10 to 500 Hz, single-channel data from 1995 varied in frequency content but was 10 to 70 Hz on the line over Site 1027. The 1985 multichannel lines were lower in frequency, dominantly 5 to 60 Hz, and the more recent multichannel line, MGL1112-02, had a broader bandwidth, 5 to 125 Hz. Single-channel data were not migrated whereas the multichannel data were.

METHODS: TIME AND DEPTH

Velocity logs were not run in Site 1027, so we used the sediment-basement reflections as ground truth to relate drilled depth below seafloor to time in the reflection section. We tested two independently derived velocity functions (Fig. 2a). For this study, Site 1027, with the deepest basement of the suite of drillholes, is the key location for fossil identifications (Su et al., 2000) and lithological descriptions (Shipboard Scientific Party, 1997b; Underwood et al., 2005).

Basement reflections provide a way to ground truth the time-depth relationship. Theoretically the high velocity–density contrast provides a high-amplitude reflection; in reality the sediment-basalt interface was complex locally and generated a suite of reflected and scattered seismic energy. At Site 1027, 569 m of sediments were drilled in hole 1027B before encountering basalt talus; 50 m away, in hole 1027C, a 10 m thick diabase sill was encountered at a depth of 585 m, 12 m above pillow basalts of the uppermost igneous crust. Basement reflections in the section are seen from 4.18 to 4.4 s two-way time (Fig. 2b). The section has not been migrated, so diffractions from adjacent basalt reflectors are contributing to the spread; small-scale roughness can also scatter sound waves. The time spread of reflected energy can also be attributed to lateral variability in depth of the basalt within the first Fresnel zone. This reflection profile is dominantly 10 to 70 Hz resulting in lateral resolution (first Fresnel zone diameter, Sheriff, 1977) of 560 to 1480 m. In addition vertical variability from talus and a sill above the pillow basalts contributed to the complex of reflections as each interface generated reflections recorded in the section. The vertical resolution near basement (1/8 wavelength assuming

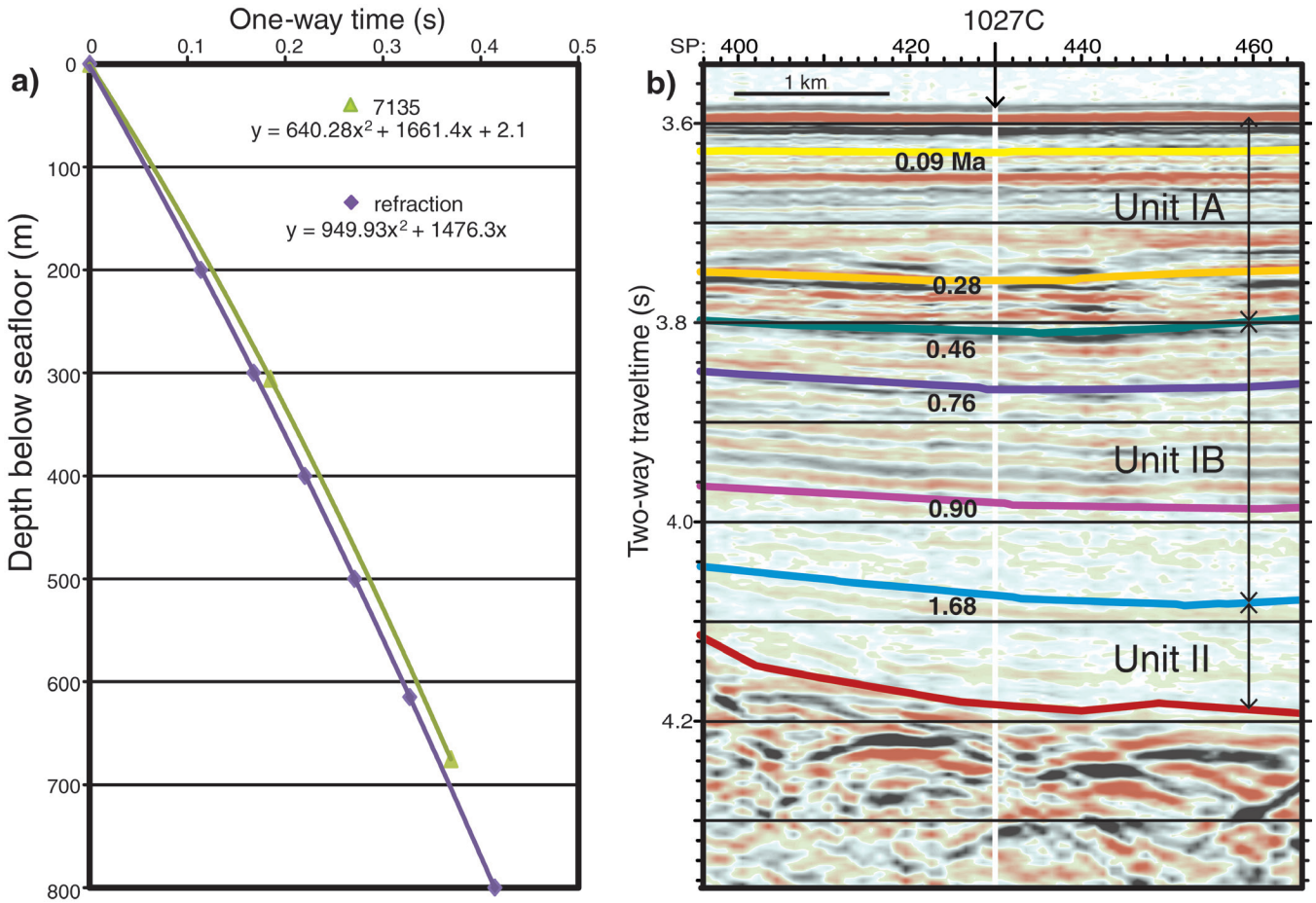

Figure 2. Correlation of depth to time. **a)** Depth below seafloor vs. one-way traveltime constructed from interval velocities from a nearby multichannel reflection line (green) (Davis et al., 1992) and from a velocity gradient (0.6 km/s/km) (purple) determined by a refraction study on the Juan de Fuca plate (Horning et al., 2016). The velocity function from cdp 7135, line 89–15 (Rohr et al., 1992) can be fit with a polynomial: $y = 640.28x^2 + 1661.4x + 2.1$ and the gradient from a refraction study can be fit with a polynomial: $y = 949.93x^2 + 1476.3x$. **b)** Seismic reflection profile across ODP site 1027C (Shipboard Scientific Party, 1997b). Ages were determined by Su et al. (2000) from cores; core depths were translated into time using the refraction formula shown in a). Lithological units IA, IB and II were interpreted by the Shipboard Scientific Party (1997b).

sediment velocity of 2500 m/s) is 3 to 31 m. The number of interfaces that occur in the gradation of basalt talus to sill to solid basalt over 37 m vertically is unlikely to be resolvable. We used the shallowest occurrence of basalt at 569 m as the likely origin of the shallowest 'basement' reflections in the section; they begin 0.6 s two-way time below seafloor.

Common depth point 7135 from multichannel line 89-15 (Fig. 1) is in the same valley as Site 1027 and 2.4 km away. Two interval velocities were computed for the sediments when the line was processed (Rohr et al., 1992); interval velocity values midway through each layer were used to construct a velocity gradient. An interval velocity vs. depth below seafloor (bsf) was converted to depth bsf vs. one-way time bsf. Likewise, we computed a curve from a velocity gradient of 0.6 km/s/km (Horning et al., 2016) and a value at the seafloor of 1700 m/s; it is very similar to the curve from interval velocities (Fig. 2a). A quadratic polynomial was fit to each set of points. Using the refraction curve, a sedimentary thickness of 558 m was derived from the one-way traveltime of 0.3 s; similarly, the interval velocity curve predicted a thickness of 528 m. The predicted depth from the refraction gradient is only 11 m too shallow, so we used that formula to convert depths in the drill core to time using this time-depth relationship.

To check our use of the refraction function, we correlated the depth of the 0.76 Ma nannofossil event in the core to reflection data at ODP Site 1032 (Shipboard Scientific Party, 1997c), which is approximately 30 km west of Site 1027. Both velocity and density logs were run from 75 to 320 m allowing a synthetic seismogram to be constructed. It matched the reflection data from 75 to 200 m, but below this, large reflections were predicted that did not match the data (Shipboard Scientific Party, 1997c). This was attributed to inaccurate log values because of 'unfavourable hole conditions'. The 0.76 Ma event was identified at 228 m (Su et al., 2000) and in spite of the inaccurate values from

200 to 228 m, we used the log to compute an arrival time for this horizon: 0.282 s bsf. In comparison the refraction function predicted a time of 0.262 s bsf. Considering the errors in both velocity functions, the 20 ms difference is acceptable. It lends confidence to our identification of this correlative time horizon in Site 1027.

We also obtained a good tie from ODP Site 888 (Fig. 1) in spite of the fact that sedimentation rates were high close to the deformation front (Shipboard Scientific Party, 1994) and one would expect sediment velocities to be lower than those predicted by the refraction gradient. A synthetic seismogram computed that the base of Unit II is at 0.515 s bsf (Shipboard Scientific Party, 1994) and the refraction function predicted this boundary at 457 m bsf would correspond to 0.5 s bsf, a difference of 15 ms.

RESULTS AND INTERPRETATION

Horizons associated with six biostratigraphic events (Su et al., 2000) were identified in the refection line (Shipboard Scientific Party, 1997b; Rosenberger et al., 2000) that crosses Site 1027; the nannofossil events span from 1.68 to 0.09 Ma (Fig. 2b). The correlative acoustic horizons can be interpreted in the valley that the site is in, but only the horizons in the Nitinat fan can be interpreted beyond the valley-defining ridges. The 0.76 Ma horizon, the base of the fan, skims the top of the ridges and can be reasonably well correlated across the ridge crests.

Tie at 1027

The hemipelagic to calcareous mud in lithological unit II (Shipboard Scientific Party, 1997b) lies between basement and the 1.68 Ma horizon; it is largely seismically transparent (Fig. 2b). Su et al. (2000) identified the top of the Pliocene less than 10 m below the 1.68 Ma event depth, which indicates an extraordinarily thin section representing the early Quaternary, 2.6 to 1.68 Ma. Between 1.68 and 0.9 Ma nearly 100 m of silty turbidites and hemipelagic mud were deposited; they also have little reflectivity. Coherent low-frequency reflectors characterize the acoustic interval with age picks between 0.9 and 0.76 Ma. The only obvious lithological differences seen in the cores between these units and those below are some thicker intervals of hemipelagic mud and 'erratic increases' in calcareous nannofossils. The 0.76 Ma nannofossil event is within lithological unit IB; above it, the cycles of hemipelagic mud and turbidite layers are more closely and regularly spaced. The 0.46 Ma nannofossil event is 16 m below the transition to subunit IA where sandy intervals and debris flows are present; this transition corresponds to a marked increase in reflection amplitudes. The 0.28 Ma nannofossil event lies just below a 30 m thick, poorly recovered interval, which has been interpreted to be primarily unconsolidated sand. Laterally across the reflection section, the acoustic horizon is irregular and above it, there is a weakly reflective to chaotic zone. The nannofossil event dated as 0.09 Ma lies in a transparent acoustic layer just 45 m below the seafloor.

Line Ties

Reflectors identified in seismic reflection data over the drill site were correlated from single-channel reflection lines collected in 1988 and 1995 to the multichannel lines.

The shortest tie is from the line across Site 1027 to scanned line 8809-23, to MGL1211-02 and then to 85-09, thus tying in two multichannel profiles (Fig. 3a). The variety of source signatures in the data results in fairly different looking sections; ties rely on matching time as well as reflection character at each juncture of two lines. For example, the transparent layer above the 0.28 Ma acoustic age pick in 950813e is similar to that in MGL1211-02, but appears more reflective in the higher frequency data in 8909-23. The 0.28 Ma acoustic horizon occurs well above the ridges; it varies in seismic character and depth, and appears to be an erosional unconformity in places. The 0.09 Ma acoustic horizon could only be interpreted on the abyssal plain; in the mid-fan, sediments are too variable in attitude to interpret this horizon confidently. Horizons from the Nitinat fan (purple horizon and above) can generally be tracked, but it is difficult to track older horizons across the basement ridges (Fig. 3a, 8.4–15.1 km offset). This composite line is oblique to the edge of the fan (Fig. 1) which results in a noticeable thickening of the uppermost sediments and shallowing of the seafloor toward the local fan apex in MGL1211-02 (Fig. 3a, 28–32 km). A channel from the fan can be seen at the very eastern end of the line in 85-09 (Fig. 3a, 36–38 km). Vancouver sea valley is evident as a slight depression in the seafloor between 1 and 11 km. Faults in MGL1211-02 were slightly modified from interpretations by Han et al. (2016).

The tie from 1027C to 85-07 (Fig. 3b and c) used lines that extend to the northwest (Fig. 1). In lines across the valley (from 0 to 32 km in Figure 3b) where Site 1027 was drilled, the oldest horizons were recognized, but beyond that only the 0.76 Ma acoustic horizon was interpreted. This horizon skims across the top of the basement ridges and can be reasonably well identified along 8809-19 and 8809-16 up to 85-07. Varying this reflector's pick by one wavelength shallower at a ridge crossing results in a ~100 ms difference in time of the reflector near the Cascadia deformation front. West of the valley containing Site 1027 the laterally irregular deposits above the interpreted 0.28 Ma horizon change to a suite of layered subparallel reflectors, indicating a change in depositional processes.

Multi-channel lines

Interpreted biostratigraphic and lithostratigraphic horizons in the regional multichannel seismic reflection lines show bending of the Juan de Fuca plate and thickness of

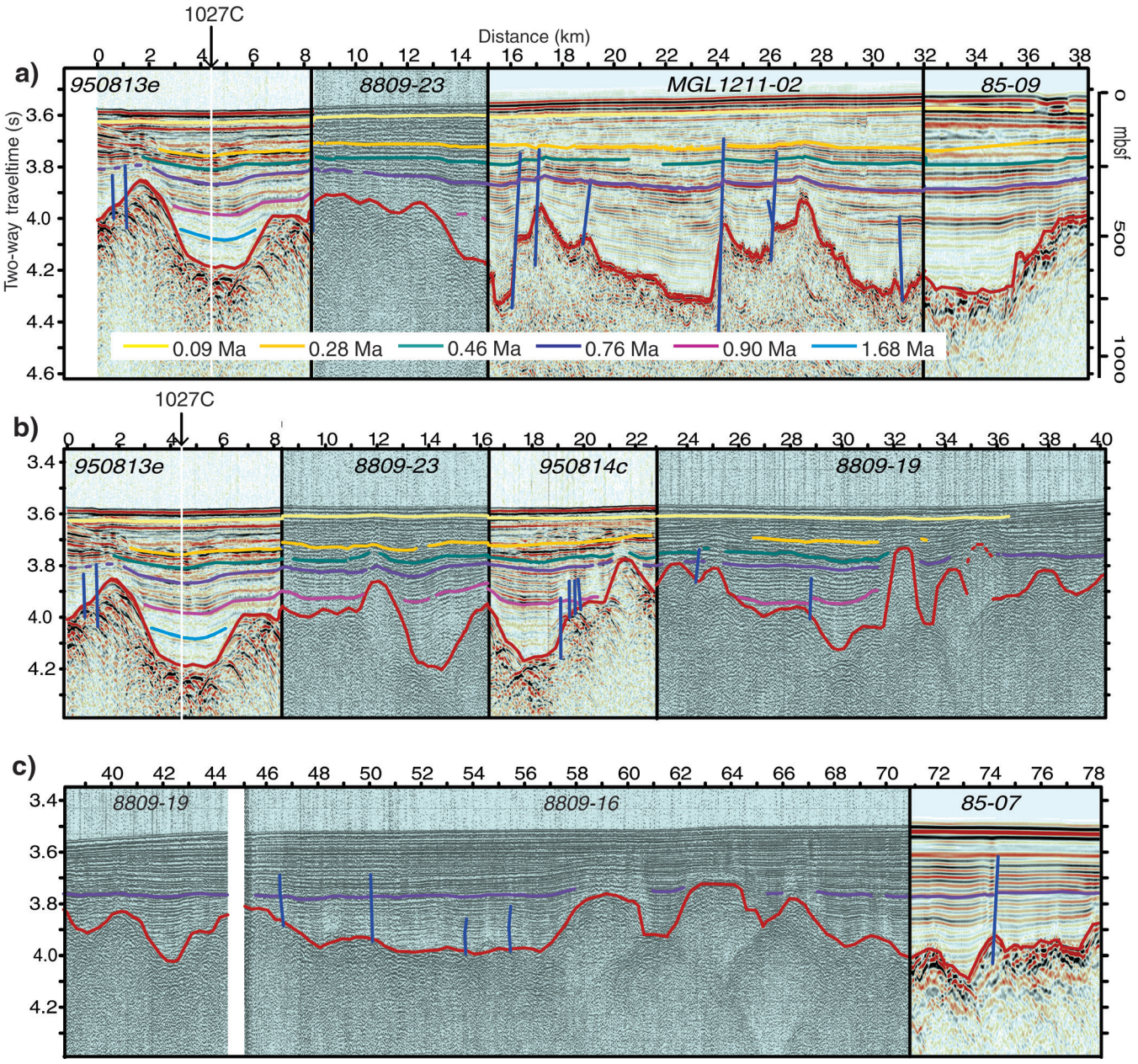

Figure 3. Ties of seismic reflection lines from ODP site 1027 to multichannel seismic reflection lines; locations are shown in Figure 1. Vertical exaggeration is ~10:1. **a)** tie to the southeast from site 1027 to MGL1211–02 and 85–09. **b)** and **c)** tie to northwest from site 1027 to 85–07; b) and c) overlap between 38 and 40 km.

the Nitinat fan deposits. From north to south, the lines cross progressively older crust; the greatest amount of bending is seen in the youngest line (85-07_85-02, Fig. 4a). It is also evident that sediments in the trench are younger than previously interpreted (Davis and Hyndman, 1989).

Only the inferred 0.76 Ma horizon was interpreted through to combined line 85-07_85-02 (Fig. 4a). It is 230 to 260 ms (~200–225 m) below the seafloor between 45 and 70 km; from there it deepens eastward toward North America. In the trench this horizon separates transparent to low-amplitude reflectors below and a wedge of more reflective layers above. Given the position of this line, these high amplitude, continuous reflectors are probably associated with thin distal turbidites, sourced from the northwest as well as from the Nitinat fan (Fig. 1).

In line 85-09_85-01 (Fig. 4b), the Nitinat fan created a rise of the seafloor between 140 and 180 km; the ~40 m deep trough (180–200 km) seaward of the deformation front is a low between a depositional lobe of the Nitinat fan and an anticline above a small thrust fault (200 km). The 0.76, 0.46, and 0.28 Ma age picks were interpreted from the tie with line MGL1211-02 (Fig. 3a and 4b). As sediments thicken into the trench, the acoustic horizon dated as 0.28 Ma bifurcates into two waveforms; the upper reflection

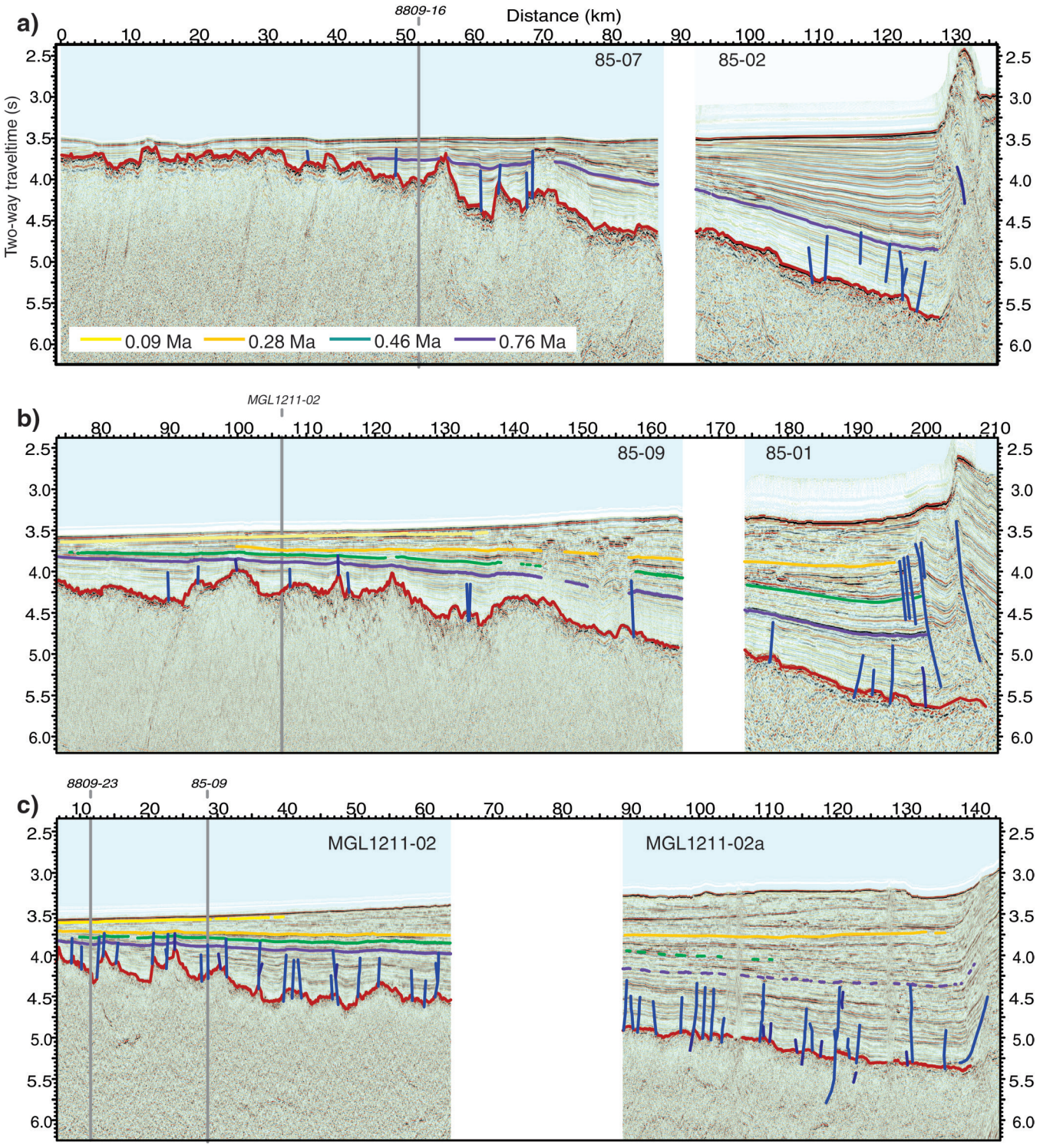

Figure 4. Regional multichannel seismic reflection profiles from mid-plate to trench. In each case only 140 km of the line is shown. Locations of profiles are shown in Figure 1. **a)** 85–07 – 85–02, **b)** 85–09 – 85–01, **c)** MGL1112–02. Gaps between displayed data are areas of no acquisition. Blue lines are faults; and oceanic basement is red. Interpretations of faults and basement in c) are after Han et al. (2016). Locations of tie lines are shown as grey vertical lines. Vertical exaggeration is ~13:1. Data shown in a) and b) were scaled with a 1000 ms automatic gain-control filter whereas the downloaded data in c) were already scaled with a 500 ms automatic gain-control filter.

is the base of a low-amplitude disturbed reflection section, and the lower reflection, while still low amplitude, is more coherent. These waveforms were tracked through a single-channel line to multichannel line 89-04 (Hyndman et al., 1994) which crossed the location of ODP Site 888 (Shipboard Scientific Party, 1994). From a synthetic seismogram based on velocity and some density measurements, the upper reflection corresponds to the transition between lithological Units II and III at 457 m bsf (Shipboard Scientific Party, 1994). Unit II is dominantly sand and had poor core recovery. This matches the description of sediments above the 0.28 Ma nannofossil event in Site 1027, so we identified the upper waveform as the equivalent horizon. Marine Isotope Stages have been identified in the upper sediments of Unit I (Knudsen and Hendy, 2009): 118 m bsf and 157 m bsf correspond to 74 ka BP and 130 ka BP, respectively. The very sandy Unit II was interpreted to have a greater deposition rate than Unit I (Shipboard Scientific Party, 1994), so our interpretation that the base of Unit II corresponds to 0.28 Ma is plausible.

Between the 0.76 Ma acoustic horizon and the seafloor, reflection amplitudes increase toward the continental slope, possibly because coarser grained material is incorporated into deposits, and the impedance contrast increases. Reflections are low amplitude above the 0.76 Ma acoustic horizon, high amplitude and continuous between the 0.46 Ma and the 0.28 Ma horizons, and very low amplitude and intermittent above the 0.28 Ma horizon. This change of character is similar to that seen in data over Site 1027: a vertical succession of weakly reflective silty turbidites, more-reflective sandier deposits above the 0.46 Ma horizon, and the variably reflective, coarse-grained turbidites and debris flows above the 0.28 Ma horizon.

Line MGL1211-02 (Fig. 4c) (Han et al., 2016) crosses the southern end of the Nitinat fan; the topography of the fan and a narrow trough just seaward of the deformation front are evident in the bathymetry map (Fig. 1). This trough corresponds to a channel which has been mapped in multibeam data. Correlating acoustic horizons across the 25 km data gap was a bit problematic. Basement has a fairly uniform dip along the line, so a simple projection of the reflectors' dip as well as seismic character were used to estimate location of horizons. Reflections above the acoustic horizon dated as 0.28 Ma are variable in attitude; they are progradational, folded, or contorted and are interspersed with locally high-amplitude continuous reflectors. Below this horizon reflections are generally continuous if variable in amplitude; distorted reflection geometries occur locally. Most of the present-day channel-levee complexes in the Nitinat fan extend in southwesterly directions from the fan apex (Fig. 1); the variability in seismic character in line MGL1211-02 may indicate that in the past channels flowed in the same direction. Below the acoustic horizon dated as 0.76 Ma a transparent layer is underlain by continuous, if faulted reflectors.

Sediment thickness and deposition rates

Using the generalized refraction gradient we can estimate sediment thicknesses and then average deposition rates. In the mid-trench, approximately 40 km from the deformation front, the total sediment thickness on lines 85-07, 85-09, and MGJ 1211-02a are 1062 m, 1520 m, and 1750 m, respectively. Closer to the deformation front, sediment seismic velocities can be affected by fluid flow from the accretionary prism (Han et al., 2017) so we restricted our computations to the mid-trench. Average deposition rates for the entire time interval before the Nitinat fan was initiated (0.76 Ma) were 178, 155 and 120 m/Ma on lines 85-07, 85-09, and MGJ 1211-02a, respectively, assuming that deposition began as soon as the igneous crust formed. However, significant depositional hiatuses were found in all drill sites across the Juan de Fuca plate ranging in duration from 0.1 to >1.5 Ma (Su et al., 2000). Assuming a hiatus of 1 Ma, the average deposition rates would then be 256, 203, and 139 m/Ma, respectively. After the fan was initiated, average deposition rates increased to 641, 1133, and 1160 m/Ma, respectively; this is an increase by factors of 2.5, 5.6, and 8.3. The highest rates are found, not surprisingly, in the mid-fan locations. With the prevalence of mass transport deposits after 0.28 Ma, deposition rates increased to ~1630 m/Ma on lines 85-01 and MGL1211-02a, which is about three times the rate for the same time interval in the mid-plate.

At Site 1027C, deposition rates generally increased over time (Su et al., 2000). From 1.68 to 1.15 Ma rates were approximately 100 m/Ma and increased to 450 to 550 m/Ma over the last 0.28 Ma. One anomalous interval stands out. Between 0.9 and 0.76 Ma the deposition rate accelerated to 740 m/Ma; no explanation has been offered for this anomaly (Su et al., 2000). The oldest possible age of initiation of the Nitinat fan is 1.06 Ma based on a date of volcanic dams across the Fraser River (Andrews et al., 2012). As the new river excavated a new bed, if not established an equilibrium profile, it may have resulted in such very high deposition rates on the seafloor. On the other hand, deposition rate may have increased if flows were confined to the valley and did not spread across the entire abyssal plain.

DISCUSSION AND SUMMARY

By tying a drillhole in central Juan de Fuca plate that is ~100 km from the deformation front to regional seismic reflection lines that cross the deformation front of the Cascadia subduction zone, we have demonstrated that much of the sediment in the trench is younger than 0.76 Ma. One ODP site in the trench, 888, could only specify that the upper 600 m of sediments were less than 0.78 Ma from paleomagnetic measurements (Shipboard Scientific Party, 1994). Previously, in the absence of paleontological dates, sediments in the trench had been dated on the basis of the character of reflectivity in seismic reflection data (Davis and Hyndman, 1989). Low-reflectivity sediments

above basement were identified as Neogene hemipelagic sediments deposited right after crustal formation and the overlying higher reflectivity sediments were considered to be Quaternary (~2.6 – 0.0 Ma). In contrast, our interpretations relate the up-section change in reflection character on line 85-01 to initiation of the Nitinat fan around 0.76 Ma (Andrews et al., 2012).

In data examined here, the character of the reflection records is consistent with a transition from sedimentary deposits with a high percentage of hemipelagic muds to younger deposits that consist of turbidites interlayered with hemipelagic muds, as noted by a number of studies (e. g. Davis and Hyndman, 1989; Underwood et al., 2005; Zühlsdorff et al., 2005). Layers with low-amplitude reflectors transition upward to more reflective layers. At Site 1027, an increase in sedimentation rate accompanied the presence of coarser turbidite deposition and later, debris flows (Shipboard Scientific Party, 1997b). Reflective layers above the acoustic horizon dated as 0.76 Ma correspond to deposition of more frequent turbidites and later, coarser turbidites; initiation of the Nitinat fan has been dated as younger than 1.06 Ma based on volcanic dams on land and likely 0.76 Ma from sediments in Sites 1027 and 888 (Andrews et al., 2012). Given the high sedimentation rate and high-amplitude reflectors between the 0.9 and 0.76 Ma age picks, the older date of 0.9 Ma could mark the initiation of the fan. Unfortunately, compartmentalization of these sediments render a regional interpretation of this horizon impossible. As the plate moved closer to the sedimentary source, coarser grained sediments and debris flows were deposited more frequently. In addition, the fan has been building out onto the plate even as its proximal end is deformed and incorporated into the Cascadia accretionary prism.

Coarser grained, high-energy deposits with common debris flows younger than 0.28 Ma were observed at Site 1027; regional seismic reflection lines show that the corresponding seismic facies occurs around and under the Nitinat fan (Fig. 5). In our interpretation the very sandy layers of Unit II in Site 888 are the same facies. In the trench this facies is up to 450–560 m thick (Fig. 4b and c) and is not confined to a single channel or sea valley. To the north, in line 85-07 the Vancouver sea valley is underlain by layered subparallel deposits (Fig. 4a (75–85 km) and Fig. 5) that interfinger to the northeast with other layered deposits. They are distinct from the coarse-grained facies observed closer to the fan and likely originate from other sedimentary sources from the north and northwest. Underwood et al. (2005) and Zühlsdorff et al. (2005) interpreted that the coarse sands drilled in Site 1027 above the 0.28 Ma horizon originated from a proto-Vancouver sea valley because the site lies underneath that valley. However, given the layered nature of the Vancouver sea valley upstream and the distribution of the coarse-grained, high-energy deposits, we infer that these sand layers originated from the Nitinat fan and/or Barkley Canyon.

Faults due to cooling and bending stresses (Han et al., 2016) are predominantly below the 0.76 Ma horizon (Fig. 4). Pre-Nitinat fan hemipelagic muds and fine-grained distal turbidites were deposited at lower rates than the fan deposits (Su et al., 2000). Offsets on these faults are typically small: 20 m and less (Han et al., 2016) and decrease up-section making these growth faults. The high sedimentation rates of fan deposition is likely overwhelming the smallest, most recent offsets that might have occurred in the shallowest section (Nedimović et al., 2009; Han et al., 2016).

Above the youngest crust in line MGL1211-02 (10–40 km) faults penetrate up to the interpreted 0.46 and 0.28 Ma horizons. In this more distal position relative to the Nitinat fan average deposition rates were 190 m/Ma between the 0.46 and 0.76 Ma horizons and 290 m/Ma between the 0.28 and 0.46 Ma horizons, respectively. Above the 0.28 Ma horizon where faults were not observed, the rate increased to 460–560 m/Ma; this rate may have been enough to overwhelm small recent offsets. We also note significant differences between porosity of the two major units in Site 1027: porosity in silt and mud below 250 m (0.76 Ma) decreased linearly from roughly 60% to 40% over 325 m (Shipboard Scientific Party, 1997b), whereas porosity in the top 100 m of sandy fan deposits interlayered with mud vary from 30 to 60% over distances of metres. Similar differences in mechanical properties could be affecting how the sediments fracture in response to small offsets from bending stresses of both the sediment load and subduction.

More faults have been interpreted in line MGL1211-02 (Fig. 4c) than in the other two lines; the higher frequency content of this data (5–125 Hz compared to 5–62.5 Hz) has provided better identification of these small offset faults. In addition, if the faults are parallel to pre-existing normal faults in oceanic crust as hypothesized by Nedimović et al. (2009), the strike of this line (perpendicular to the faults) would cross more faults than lines oriented more obliquely, such as the other two multichannel lines.

As a first attempt at extending acoustic stratigraphy from mid-plate to the deformation front, the generalized velocity function we used has been serviceable. As described above, at ODP sites 1032 and 888 comparing two-way traveltime to a depth horizon predicted by this function yielded a number within 20 and 16 ms of calculated synthetic seismograms from depths of 228 and 457 m bsf, respectively. In practice, the velocity function only had to be reliable at Site 1027 to allow correlation between the depths of biostratigraphic events in cores to reflections in seismic data across that site. Obtaining accurate velocity data over Site 1027 and a single seismic reflection survey connecting this location to regional multichannel lines would refine our interpretations. Accurate velocity profiles throughout the basin would allow for more accurate sediment thicknesses and deposition rates to be calculated; this is especially important in the trench where deposition rates increase landward.

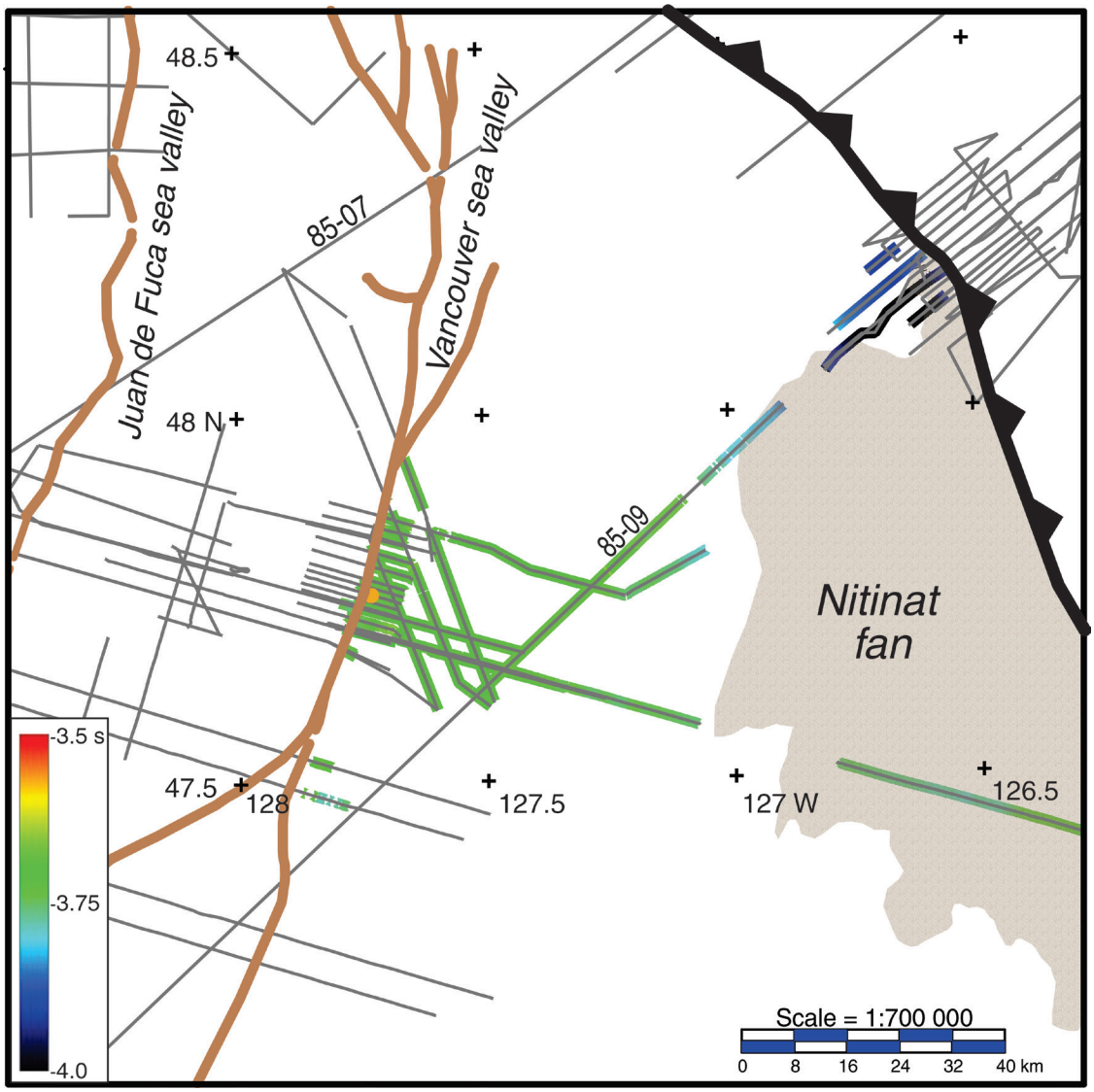

Figure 5. Observations of the 0.28 Ma horizon are located around and under the Nitinat fan. Coloured lines show time to the horizon; it deepens from 3.73 to 3.93 near the deformation front (thick black line). Grey lines show locations of seismic reflection data in the region. Vancouver and Juan de Fuca sea valleys are shown as brown lines; on the seafloor they are both about 10 km wide. Extent of the Nitinat fan was picked as a generalized 2500 m bathymetric contour. ODP Site 1027 is shown as a yellow dot. The subduction zone is indicated by thick black line.

Sedimentation rate affects thermal structure of the subducting slab (e.g. Wang and Davis, 1992; Rotman and Spinelli, 2013) because hydrothermal circulation in permeable basalt cools the plate until sediments are thick enough to seal the crust hydrologically above topographic basement highs (i.e. potential zones of recharge and discharge). Accurate calculations of this effect rely on knowledge of what kind of sediments were deposited and at what rates and how these factors varied over time. To date thermal models of the slab have used the older dates (Davis and Hyndman, 1989) to estimate sedimentation rates (e.g. Hyndman and Wang, 1993). From previous knowledge of sedimentary hiatuses (Su et al., 2000) and our results, we now know that these rates are too slow and that they predict a time of hydrological sealing that is too old.

Given the younger time of fan deposition, the northeastern Juan de Fuca plate could have been exposed to ventilated hydrothermal circulation for ~1 to 2 Ma longer than previously interpreted. Using a spreading rate of ~42 km/Ma (Wilson, 2002) high sedimentation rates began when crust currently at the deformation front was ~30 km away from the trench and well within the zone of bending stresses. Small faults offset upper Juan de Fuca crust and sediments up to 200 km away from the trench (Nedimović et al., 2009).

If they pierced the seafloor prior to 0.76 Ma and had sufficient fault permeability, they could have acted as conduits for water into upper oceanic crust. This would affect thermal structure of uppermost levels of the subducted plate presently under the continental slope and shelf where the active thrust fault between North America and the Juan de Fuca plate under Vancouver Island is interpreted to lie (Davis and Hyndman, 1989). Presently, the depth to which significant cooling of the igneous crust takes place is poorly resolved.

Depositional history, compaction dewatering, and thermally driven diagenetic dehydration reactions are important factors in determining pore-fluid pressure throughout the sedimentary section, which in turn affects location of the megathrust interface, its physical properties and therefore, slip behaviour (e.g. Yuan et al., 1994; Han et al., 2017). Over what depth range ruptures occur along the megathrust, and whether they extend up to the seafloor, are significant questions that affect estimates of hazards from tsunamis triggered by megathrust events (Wang and Trehu, 2016). Results presented here allow more reliable estimates of megathrust rupture to be made; they could be further refined by good velocity data at Site 1027 and a regional reflection survey that tied this site to multichannel seismic reflection data.

ACKNOWLEDGMENTS

Special thanks to R. Ferguson, T. Brent and the team of scientists who worked on the Pacific Basin Conservation Zone Assessment; compiling reflection data for the region has resulted in an invaluable resource. Thanks also to Earl Davis, Jim Dietrich, Randy Enkin, Shuoshuo Han, Michael Underwood, and Stefan Wenau who reviewed and helped improve the manuscript. The 1985 data are available from Natural Resources Canada: https://open.canada.ca/data/en/dataset/eca7a8a7-4f26-4408-8036-c1e9adfd5585 .

The 1988 data are also available from Natural Resources Canada: http://ftp.maps.canada.ca/pub/nrcan_rncan/raster/marine_geoscience/Seismic_Reflection_Scanned/NRCan_Seismic_Reflection_Scanned.kmz. The 1996 and 1998 data are available at Ocean Drilling Program data repository: https://ssdb.iodp.org/SSDBquery/SSDBquery.php. The R/V Marcus G. Langseth data collected in 2012 are available from the Academic Seismic Portal at UTIG, Marine Geoscience Data System. http://dx.doi.org/10.1594/IEDA/500069

REFERENCES

Andrews, G.D.M., Russell, J.K., Brown, S.R., and Enkin, R.J., 2012. Pleistocene reversal of the Fraser River, British Columbia; Geology, v. 40, p. 111–114. https://doi.org/10.1130/G32488.1

Davis, E.E. and Hyndman, R.D., 1989. Accretion and recent deformation of sediments along the northern Cascadia subduction zone; Geological Society of America Bulletin, v. 101, p. 1465–1480. https://doi.org/10.1130/0016-7606(1989)101%3c1465:AARDOS%3e2.3.CO%3b2

Davis, E.E., Chapman, D.S., Mottl, M.J., Bentkowski, W.J., Dadey, K., Forster, C., Harris, R., Nagihara, S., Rohr, K., Wheat, G., and Whiticar, M., 1992. FlankFlux: an experiment to study the nature of hydrothermal circulation in young oceanic crust; Canadian Journal of Earth Sciences, v. 29, p. 925–952. https://doi.org/10.1139/e92-078

Ewing, J., Ewing, M., Aitken, T., and Ludwig, W.J., 1968. North Pacific sediment layers measured by seismic profiling; in The Crust and Upper Mantle of the Pacific Area, (ed.) C.L. Knopoff, P. Drake, and J. Hart; American Geophysical Union, Geophysical Monograph Series, 12L, p. 147–173.

Ferguson, R., King, H., Kublik, K., Rohr, K., Kung, L., Lister, C.J., Fustic, M., Hayward, N., Brent, T.A., and Jassim, Y., 2018. Petroleum, mineral and other resource potential in the offshore Pacific, British Columbia, Canada; Geological Survey of Canada, Open File 8390, 82 p. https://doi.org/10.4095/308395

Gardner, J.V., Cacchione, D.A., Drake, D.E., Edwards, B.D., Field, M.E., Hampton, M.A., Karl, H.A., Kenyon, N.H., Masson, D.G., and McCulloch, D.S., 1993. Map showing sediment isopachs in the deep sea basins of the Pacific Continental Margin, Strait of Juan de Fuca to Cape Mendocino; United States Geological Survey, Miscellaneous Investigations Series Map 1- 2091-A, scale 1:1 000 000.

Griggs, G.B. and Kulm, L.D., 1973. Origin and development of Cascadia deep-sea channel; Journal of Geophysical Research, v. 78, p. 6325–6339. https://doi.org/10.1029/JC078i027p06325

Hampton, M.A., Karl, H.A., and Kenyon, N.H., 1989. Sea-floor drainage features of Cascadia Basin and the adjacent continental slope, Northeast Pacific Ocean; Marine Geology, v. 87, p. 249–272. https://doi.org/10.1016/0025-3227(89)90064-9

Han, S., Carbotte, S.M., Canales, J.P., Nedimović, M.R., Carton, H., Gibson, J.C., and Horning, G.W., 2016. Seismic reflection imaging of the Juan de Fuca plate from ridge to trench: new constraints on the distribution of faulting and evolution of the crust prior to subduction; Journal of Geophysical Research, v. 121, p. 1849–1872. https://doi.org/10.1002/2015JB012416

Han, S., Bangs, N.L., Carbotte, S.M., Saffer, D.M., and Gibson, J.C., 2017. Links between sediment consolidation and Cascadia megathrust slip behavior; Nature Geoscience, v. 10, p. 954–959. https://doi.org/10.1038/s41561-017-0007-2

Hasselgren, E.O. and Clowes, R.M., 1995. Crustal structure of northern Juan de Fuca plate from multichannel reflection data; Journal of Geophysical Research, v. 100, p. 6469–6486. https://doi.org/10.1029/94JB02941

Hayes, D.E. and Ewing, M., 1970. Pacific boundary structure; *in* The Sea, v. 4, The Earth Beneath the Sea - Concepts, pt. 2, Regional Observations, (ed.) A.E. Maxwell, Wiley-Interscience, New York, p. 29–72.

Horning, G., Canales, J.P., Carbotte, S.M., Han, S., Carton, H., Nedimović, M.R., and van Keken, P.E., 2016. A 2-D tomographic model of the Juan de Fuca plate from accretion at axial seamount to subduction at the Cascadia margin from an active source ocean bottom seismometer survey; Journal of Geophysical Research, v. 121, p. 5859–5879. https://doi.org/10.1002/2016JB013228

Hyndman, R.D. and Wang, K., 1993. Thermal constraints on the zone of major thrust earthquake failure: The Cascadia subduction zone; Journal of Geophysical Research, v. 98, p. 2039–2060. https://doi.org/10.1029/92JB02279

Hyndman, R.D., Spence, G.D., Yuan, T., and Davis, E.E., 1994. Regional geophysics and structural framework of the Vancouver Island margin accretionary prism; *in* Proceedings Ocean Drilling Program, Initial Reports, (ed.) G.K. Westbrook, B. Carson, and R.J. Musgrave; Ocean Drilling Program, v. 146, College Station, Texas, p. 399–419. https://doi.org/10.2973/odp.proc.ir.146-1.002.1994

Karl, H.A., Hampton, M.A., and Kenyon, N.H., 1989. Lateral migration of Cascadia channel in response to accretionary tectonics; Geology, v. 17, p. 144–147. https://doi.org/10.1130/0091-7613(1989)017%3c0144:LMOCCI%3e2.3.CO;2

Knudsen, K.P. and Hendy, I.L., 2009. Climatic influences on sediment deposition and turbidite frequency in the Nitinat Fan, British Columbia; Marine Geology, v. 262, p. 29–38. https://doi.org/10.1016/j.margeo.2009.03.002

McManus, D.A., Holmes, M.L., Carson, B., and Barr, S.M., 1972. Late Quaternary tectonics, northern end of Juan de Fuca Ridge; Marine Geology, v. 12, p. 141–164. https://doi.org/10.1016/0025-3227(72)90025-4

Nedimović, M.R., Bohnenstiehl, D.R., Carbotte, S.M., Canales, J.P., and Dziak, R.P., 2009. Faulting and hydration of the Juan de Fuca plate system; Earth and Planetary Science Letters, v. 284, p. 94–102. https://doi.org/10.1016/j.epsl.2009.04.013

Prytulak, J., Vervoort, J.D., Plank, T., and Yu, C., 2006. Astoria Fan sediments, DSDP site 174, Cascadia Basin: Hf-Nd-Pb constraints on provenance and outburst flooding; Chemical Geology, v. 233, p. 276–292. https://doi.org/10.1016/j.chemgeo.2006.03.009

Riddihough, R., 1977. A model for recent plate interactions off Canada's west coast; Canadian Journal of Earth Sciences, v. 14, p. 384–396. https://doi.org/10.1139/e77-039

Rohr, K., Davis, E.E., and Hyndman, R.D., 1992. Multi-channel seismic reflection survey over the northern Juan de Fuca ridge; Geological Survey of Canada, Open File 2476, 1 .zip file. https://doi.org/10.4095/183851

Rosenberger, A., Davis, E.E., and Villinger, H., 2000. Data Report: Hydrocell-95 and –96 single-channel seismic data on the eastern Juan de Fuca ridge flank; *in* Proceedings of the Ocean Drilling Program, Scientific Results, (ed.) A.T. Fisher, E.E. Davis, and C. Escutia, Ocean Drilling Program, v. 168, College Station, Texas, p. 9–19.

Rotman, H.M.M. and Spinelli, G.A., 2013. Global analysis of the effect of fluid flow on subduction zone temperatures; Geochemistry Geophysics Geosystems, v. 14, p. 3268–3281. https://doi.org/10.1002/ggge.20205

Ryan, W.B.F., Carbotte, S.M., Coplan, J.O., O'Hara, S., Melkonian, A., Arko, R.C., Weissel, R.A., Ferrini, V., Goodwillie, A., Nitsche, F., Bonczkowski, J., and Zemsky, R., 2009. Global Multi-Resolution Topography synthe sis; Geochemistry Geophysics Geosystems, v. 10, cit. no. Q03014. https://doi.org/10.1029/2008GC002332.

Sheriff, R.E., 1977. Limitations on resolution of seismic reflections and geologic detail derivable from them; in Seismic Stratigraphy – applications to hydrocarbon exploration, Memoir, Volume 26, (ed.) C.E. Payton; American Association of Petroleum Geologists, Tulsa, Oklahoma, p. 3–14.

Shipboard Scientific Party, 1994. Site 888; *in* Proceedings Ocean Drilling Program, Initial Reports, (ed.) G.K. Westbrook, B. Carson, and R.J. Musgrave; Ocean Drilling Program, v. 146, College Station, Texas, p. 55–125. https://doi.org/10.2973/odp.proc.ir.146-1.007.1994

Shipboard Scientific Party, 1997a. Introduction and summary: hydrothermal circulation in the oceanic crust and its consequences on the eastern flank of the Juan de Fuca ridge; *in* Proceedings Ocean Drilling Program, Initial Reports (ed.) E.E. Davis, A.T. Fisher, and J.V. Firth; Ocean Drilling Program, v. 168, College Station, Texas, p. 7–21. https://doi.org/10.2973/odp.proc.ir.168.104.1997

Shipboard Scientific Party, 1997b. Rough basement transect (Sites 1026 and 1027); *in* Proceedings Ocean Drilling Program, Initial Reports, (ed.) E.E. Davis, A.T., Fisher, and J.V. Firth, Ocean Drilling Program, v. 168: College Station, Texas, p. 101–160. https://doi.org/10.2973/odp.proc.ir.168.105.1997

Shipboard Scientific Party, 1997c. Buried basement transect (Sites 1028, 1029. 1030, 1031, and 1032); *in* Proceedings Ocean Drilling Program, Initial Reports, (ed.) E.E. Davis, A.T., Fisher, and J.V. Firth, Ocean Drilling Program, v. 168: College Station, Texas, p. 161–212. https://doi.org/10.2973/odp.proc.ir.168.106.1997

Su, X., Baumann, K.H., and Thiede, J., 2000. Calcareous nannofossils from Leg 168: biochronology and diagenesis; *in* Proceedings Ocean Drilling Program, Scientific Results, (ed.) E.E. Davis, A.T., Fisher, and J.V. Firth, Ocean Drilling Program, v. 168: College Station, Texas, p. 39–49. https://doi.org/10.2973/odp.proc.sr.168.015.2000

Underwood, M.B., Hoke, K.D., Fisher, A.T., Davis, E.E., Giambalvo, E., Zühlsdorff, L., and Spinelli, G.A., 2005. Provenance, stratigraphic architecture, and hydrogeologic influence of turbidites on the mid-ocean ridge flank of northwestern Cascadia Basin, Pacific Ocean; Journal of Sedimentary Research, v. 75, p. 149–164. https://doi.org/10.2110/jsr.2005.012

Wang, K. and Davis, E.E., 1992. Thermal effects of marine sedimentation in hydrothermally active areas; Geophysical Journal International, v. 110, p. 70–78. https://doi.org/10.1111/j.1365-246X.1992.tb00714.x

Wang, K. and Trehu, A.M., 2016. Invited review paper: Some outstanding issues in the study of great megathrust earthquakes – The Cascadia example; Journal of Geodynamics, v. 98, p. 1–18. https://doi.org/10.1016/j.jog.2016.03.010

Wilson, D., 1993. Confidence intervals for motion and deformation of the Juan de Fuca plate; Journal of Geophysical Research, v. 98, p. 16053–16071. https://doi.org/10.1029/93JB01227

Wilson, D., 2002. The Juan de Fuca plate and slab: isochron structure and Cenozoic plate motions; in The Cascadia subduction zone and related subduction systems – seismic structure, intraslab earthquakes and processes, and earthquake hazards, (ed.) S. Kirby, K. Wang, and S. Dunlop; Geological Survey of Canada, Open File 4350, p. 9–12.

Yuan, T., Spence, G.D., and Hyndman, R.D., 1994. Seismic velocities and inferred porosities in the accretionary wedge sediments at the Cascadia margin; Journal of Geophysical Research, v. 99, p. 4413–4427. https://doi.org/10.1029/93JB03203

Zühlsdorff, L. and Spiess, V., 2001. Modeling seismic reflection patterns from Ocean Drilling Program Leg 168 core density logs: Insight into lateral variations in physical properties and sediment input at the eastern flank of the Juan de Fuca Ridge; Journal of Geophysical Research, v. 106, p. 16119–16134. https://doi.org/10.1029/2001JB900005

Zühlsdorff, L., Hutnak, M., Fisher, A.T., Speiss, V., Davis, E.E., Nedimovic, M., Carbotte, S., Villinger, H., and Becker, K., 2005. Site surveys related to IODP Expedition 301: Image-Flux (SO149) and RetroFlux (TN116) expeditions and earlier studies; *in* Proceedings of the Ocean Drilling Program, Scientific Results, (ed.) A.T. Fisher, T. Urabe, A. Klaus, Ocean Drilling Program, v. 301, College Station, Texas, p. 1–48.

Geological Survey of Canada Project SO1010-SO1